Quantum size stabilization of Ge_3Pt nanofilms on Ge(001)

Bene Poelsema, Ali Safaei, Raoul van Gastel, Harold J. W. Zandvliet, and Arie van Houselt
Physics of Interfaces and Nanomaterials, MESA + Institute for Nanotechnology, University of Twente, P.O. Box 217, 7500 AE Enschede, The Netherlands

(Received 7 January 2019; revised manuscript received 5 April 2019; published 24 June 2019)

The electronic and structural properties of a Ge-Pt alloy film on Ge(001) were studied with low-energy electron microscopy. Well above 1000 K, a bulklike eutectic film forms, followed by the emergence of an ordered Ge_3Pt alloy upon solidification, which sets in at 1004 K. This eight-layers-thick Ge_3Pt phase is remarkably robust as it is stabilized by quantum size effects. Further cooling results in the evolution of ultrathin Pt-induced nanowires around 650 K. The process is reversible upon temperature variation around the eutectic point. The results are considered representative of an important class of surface alloys.

DOI: 10.1103/PhysRevMaterials.3.065005

I. INTRODUCTION

After decades of intensive research on the structure and properties of surfaces, the knowledge of their differences with respect to bulk planes is now well established. A deviation of the interlayer spacing near the interface (relaxation) is well known especially for transition metals [1]. Also changes in the periodicity from (1×1) to higher-order (reconstructions) have become a standard topic in textbooks [2]. However, surprisingly little is yet known about the structure and properties of deeper layers and hidden interfaces, sometimes coined as "$2+1$"-dimensional structures. This knowledge originates mainly from characterization using invasive methods, such as transmission electron microscopy and cross-sectional scanning tunneling microscopy. Soft x-ray tools do offer some relief but only for homogeneous macroscopic surfaces. Unfortunately, crucial microscopic information on structure and properties of layers 2–10 is hardly available, mainly due their inaccessibility for nonintrusive surface science tools especially scanning probes.

Thin films play an important part, both in technology and in basic research. They play a crucial role in creating new mechanical, optical, electronic, chemical, and magnetic properties. We currently focus on one of the most intriguing materials: Thin films, which, in combination with the substrate material, form a binary alloy with a deep eutectic, i.e., the melting point of the alloy is well below those of both pure elements. The most important and comprehensive class of materials in this context consists, for obvious reasons, of metals with semiconductors, most notably silicon (e.g., Ref. [3]). They are also of great interest, both in curiosity and in application-driven research as exemplified by the growth of nanowires from a eutectic solution [4]. In this situation, standing-up Si nanowires are grown from a eutectic gold silicon droplet in a supersaturated silicon-containing gas phase. Another intriguing example is the formation of a Au-Si eutectic on clean Si [5–7]. For this system, the existence of a crystalline surface layer, floating on top of a liquid, was demonstrated well above the eutectic point. Here, it is important to note that the effect was found for a film thickness of about eight atomic layers, i.e., similar to the main region of interest here. We also stress that the Au-Si film was reported to be very flat [7] and its thickness larger than expected. Both features still lack a proper explanation.

An intriguing example of spontaneous hosting of self-organized nanowires (NWs) is represented by lying-down Pt-induced nanowires (PiNWs) on Ge(001). This system leads to a distinctly different class of nanowires, which consist of only one-atom-thick NWs residing on alloyed Ge(001) terraces [8,9]. Not only their width is extreme, but their length can easily surpass 100 nm as they run basically from defect to defect. They, therefore, have the largest known aspect ratios for nanoparticles. The system exhibits other interesting properties too, such as, e.g., electronic states confined between the PiNWs [10] and a Peierls transition at low temperatures [11]. The Pt-modified surface was described as inhomogeneous and consists of Pt-rich β terraces and lesser Pt-rich α terraces. The PiNWs nanowires emerge exclusively on β terraces [8]. They run along $\langle 110 \rangle$ directions with a minimum and typical separation distance of 1.6 nm. The periodicity along the wires is 0.8 nm, and they, thus, form well-ordered (2×4) domains. At temperatures above ca. 1000 K a bulklike eutectic alloy ($Ge_{1-x}Pt_x$ with $x = 0.22$) is formed. Upon cooling through the solidification transition, the PiNWs evolve by spinodal decomposition [12]. Circumstantial experimental evidence suggests that the dimers consist of Pt [11–14]. Here, we study the nature of the Ge-Pt alloy that develops from the eutectic. We argue that it exists of an ordered, several layers thick, Ge_3Pt alloy.

II. EXPERIMENTAL

Experiments have been performed in an ultrahigh vacuum low-energy electron microscope (Elmitec LEEM III). The flat Ge(001) samples ($10 \times 10 \times 0.5$ mm, n type) were mounted on a Mo holder. Contact to any other metal was carefully avoided prior to the experiments. The samples were cleaned by 600-eV Ar^+ ion sputtering and subsequently annealed at 1100 K [8]. Platinum was deposited at room temperature by evaporation from a resistively heated W wire, wrapped

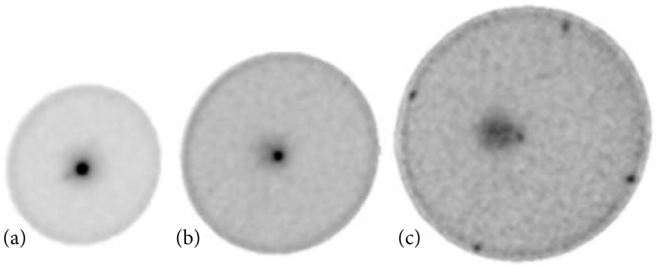

FIG. 1. Inverted LEED patterns obtained at 1006 K with (a) 4.3-eV, (b) 7.7-eV, and (c) 12.8-eV electrons. The patterns have been inverted and corrected for the secondary electron contribution.

with high-purity Pt (99.995% purity). After Pt deposition, the sample was also annealed at 1100 K. We estimate the uncertainty in the absolute temperature at about 25 K, but the relative temperature within one experiment is considered correct to ±1 K. We have calibrated the deposited Pt amount with x-ray photoelectron spectroscopy (XPS) and found 1.3 monolayer equivalent (MLE). One MLE is defined as 1 Pt atom per Ge surface atom for the Ge(001) surface. The obtained Pt amount is an underestimate for two reasons. First, Pt has a strong tendency to disappear below the surface already at room temperature [15]. A similar effect holds for the formation of platinum germanide nanocrystallites on top of the surface [8,15]. These are probably Pt-rich Ge-Pt alloys, and the exact amount of Pt stored in these crystallites remains underestimated by quantitative XPS analysis too. We estimate the real total Pt coverage at 2 to 3 MLE. Finally, we note that Ge has a diamond structure with a lattice constant of 5.66 Å. The unreconstructed Ge(001) surface has a square geometry with a nearest-neighbor distance of 4.00 Å, and the interlayer distance amounts to 1.41 Å.

III. RESULTS AND DISCUSSION

Figure 1 shows LEED images obtained at 1006 K, a few kelvin above the eutectic temperature. Just the specular peak and no fractional order peaks are visible [cf. Figs. 1(a) and 1(b)]. The first-order peaks for Ge(001) emerge at 11.4 eV [cf. Fig. 1(c)]. The absence of fractional order peaks nicely confirms that the Ge-Pt alloy film has melted.

Figure 2(a) shows a characteristic dark-field [16] LEEM image of the clean Ge(001) surface after an extended period of cleaning cycles. The white areas show (2×1) reconstructed terraces, whereas the dark areas represent (1×2) dimer terminated ones [17,18]. The gray colors correspond to areas which are not resolved by LEEM, i.e., the local terraces are too narrow to distinguish between (2×1) and (1×2) (dimer) reconstructions. We refer to them as "step bunches" varying from local terrace widths below the lateral resolution of the instrument to multiple steps. Figures 2(b)–2(d) show snapshots from a bright-field LEEM movie taken during slow cooling from above the eutectic transition temperature T_C at 1006 K to below T_C [19]. It is immediately clear that the step-bunch areas are much smaller in the presence of Pt and the number of larger terraces has decreased by roughly an order of magnitude. In other words, the Pt modification leads to substantially smoother surfaces on a local scale. This is

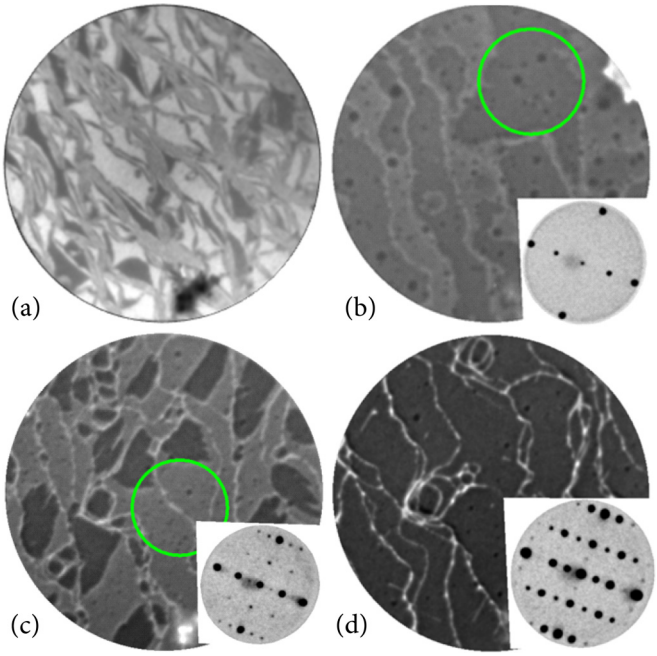

FIG. 2. (a) $(\frac{1}{2}, 0)$-beam dark-field LEEM image (2.9 eV, room temperature, field of view 6 μm) of clean Ge(001). (b)–(d) Snapshots from a (0,0)-beam bright-field movie (6-μm field of view) during cooling from 1006 to 1004 K [(b) 12 eV], 644 K [(c) 12.6 eV], and 614 K [(d) 12.5 eV]. The insets show selected area diffraction (μLEED) from the circular areas indicated in green [(b) and (c)] and the integral LEED pattern in (d).

true, even though the samples had a very similar temperature history, both in thermal and in temporal respects. This is a direct consequence of the eutectic, which has relatively high entropy, and thus strives for wetting the surface. At 1004 K, already a part of the surface layers has solidified as evidenced by the single domain (2×1) μLEED pattern of Fig. 2(b). It reflects a, compared to Ge(001), two times larger unit cell of what we propose to be, and will discuss further below, a new Ge_3Pt alloy. Note that the first-order positions in Fig. 1(c) and Fig. 2(b) and, hence, the lattice constants are identical. At 644 K [Fig. 2(c)], the PiNW formation has set in as shown by the formation of a predominantly single (4×2) domain. At 614 K [Fig. 2(d)], the NW domains have fully deployed, and the entire surface is covered by NWs. Note that PiNWs only grow on so-called β^* domains. These Pt-rich domains develop during the slow cool down after passing the eutectic transition. Less Pt-rich terraces also appear, denoted as α^* domains, represented by the step bunches. Previous studies [8–14] show that α^* and β^* domains coexist after fast cooling. The asterisks indicate that one deals with Ge-Pt alloys which extend several layers in depth (see further below) instead of a purely 2D surface (i.e., first layer) feature assumed so far.

A comparison of Fig. 2(b) with Figs. 2(c) and 2(d) shows that the step bunches appear brighter in the latter cases. This is attributed to a consequence of spinodal decomposition of the eutectic $Ge_{(1-x)}Pt_x$ with $x = 0.22$, leading to a higher Pt density in an ordered Ge_3Pt ($x = 0.25$) alloy and a lower concentration of Pt in the α^* phase at and near the step bunches. We consider the step bunches as an engine for exchange of

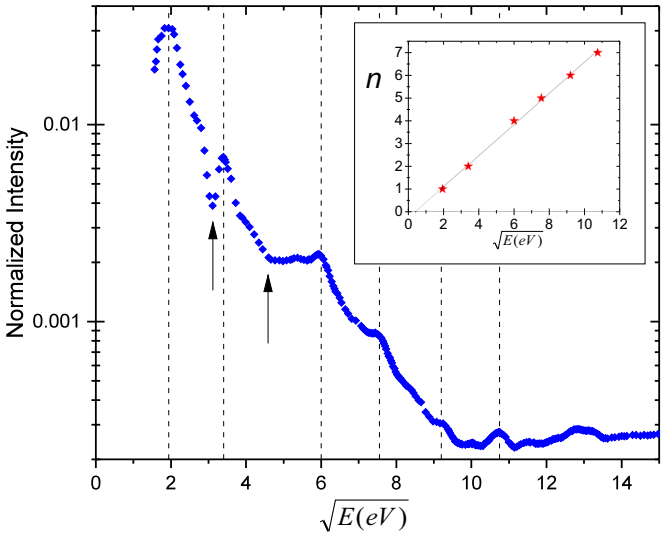

FIG. 3. Intensity versus $\sqrt{E}$ for the specular beam, measured at 641 K. The left-hand arrow corresponds to a periodicity of 4 Å and, thus, to resonant scattering via the (1,0) and (0,1) diffraction channels. The right arrow would indicate resonant scattering via the (1,1) channel. The dashed lines indicate distinct maxima on the $(I, \sqrt{E})$ curve. The sequence of these equidistant maxima is plotted in the inset except for the missing number 3.

platinum between near-surface layers. Note that the pure Ge bulk below the abrupt interface would act as the low (i.e., zero) Pt containing the phase during spinodal decomposition of the eutectic when passing the phase transition towards solidification [12,19].

Figure 3 shows the specular intensity versus $\sqrt{E}$ curve for data taken at 651 K on the bare β^* phase. The $\sqrt{E}$ scale, that differs from the source reading due to work-function differences between the source and the sample, is calibrated using the intensity dip at 9.4 eV. The pronounced minimum at 9.4 eV is at a too high energy for attribution to intensity losses due to inelastic excitations, including plasmon excitations. We rather assign the intensity loss to a natural consequence of bound-state resonances [20]. These resonances can occur when the following conditions are fulfilled:

$$E_{fn} = E_i + \varepsilon_n \quad \text{and} \quad \mathbf{k}_f - \mathbf{k}_i = \mathbf{G}_{i-f}, \tag{1}$$

in which i and f refer to initial and final states of the diffracting electron with energy and wave vector given by E and $\mathbf{k}$, respectively. $\mathbf{G}_{i-f}$ denotes the reciprocal lattice vectors involved in the diffraction process, and ε_n is the energy with respect to the vacuum level of the nth eigenstate of the image potential. For the square lattice considered here and a first-order diffraction, one obtains for the resonance condition,

$$E_i = -\varepsilon_n + \frac{h^2}{2m}\frac{1}{a_{nn}^2}, \tag{2}$$

with h as Planck's constant, a_{nn} as the nearest-neighbor distance, and m as the electron mass. Since we here consider diffraction into a channel parallel to the surface, and the incident energy is low, the electron does hardly feel the inner potential of the substrate, and for the mass of the electron, we, thus, take its rest mass m_0. For a metal, the dominant ground-state ε_1 amounts to about 0.6 eV. In the current situation, this value is even smaller due to a smaller density of charge carriers as we will see further below. The only remaining uncertainty in the absolute energy scale is the exact value of ε_n. The electron can travel along the surface below the vacuum level until it undergoes a reverse diffraction process which returns it into the specular beam. On its way along the surface, it may be scattered by defects or undergo inelastic losses, which both give rise to a loss of coherent intensity and, thus, to a minimum in the specular intensity [20]. Such processes are most prominent at low energies and during interaction with highly corrugated surfaces with an inherently high diffractive power. We used the dominant intensity dip at $E = 9.4$ eV to shift the experimental energy scale such that the main intensity dip coincides exactly with 9.4 eV, which corresponds to an electron wave length of 4 Å [cf. Eq. (2)]. Note that this distance is equal to the Ge-Ge nearest-neighbor distance and is, thus, dominantly present at the surface. The intensity dip, thus, corresponds to resonances involving integer order diffraction processes (1,0) and (0,1). Note that both domains (2×1) and (1×2) would contribute equally to intensity losses in the (0,0) beam at the same energy. The required shift amounts to 0.75 eV, which is realistic in view of the difference in work functions of a substrate, the electron source, and the position of the ground level of the image potential as mentioned above. Note that the high corrugation and the weak Debye-Waller (DW) attenuation at these low energies reinforce the occurrence of bound-state resonances.

The $(I, \sqrt{E})$ curve in Fig. 3 shows a distinct and remarkable pattern: Peaks appear at equidistant positions on the $\sqrt{E}$ scale as indicated by the dashed lines. They reveal the existence of quantum interferences. The maxima represent constructive interference conditions for electrons reflected from two plan-parallel interfaces, the buried one and the surface. The conditions for these Fabry-Pérot-type interferences are set purely by the spacing between the two interfaces, defined as the planes through the outermost Ge_3Pt atoms. For a perfectly crystalline phase with exact periodic conditions imposed by the interlayer spacing d, the distance between the two interfaces D equals $(N-1)d$ for an N-layers-thick film. (Possible phase differences upon reflection from both individual interfaces are neglected.) Then, constructive interference peaks occur for diffraction order n at energy positions E_n given by

$$E_n = \frac{n^2h^2}{8m^*D^2}, \tag{3}$$

with h as Plank's constant, E_n as the energy, and m^* as the effective mass of the electrons traveling within the crystal field of the Ge_3Pt film. The prominence of the peaks marked by the dashes decreases with increasing order n due to increasing DW attenuation and a decreasing electron mean free path. A notable exception is made for the one corresponding to the Bragg peak since, in contrast to all others, each individual $Ge_3Pt(001)$ plane contributes purely in phase. The obvious candidate is the peak with $n = 7$. It is the only one in its wider neighborhood with a maximum intensity which is, at least, 35% above the local baseline. Therefore, we select the $n = 7$ peak as the Bragg peak. From the number of peaks, one then immediately obtains the number of layers and, thus, the

thickness of the film [16,21–25]. We stress that the $(I, \sqrt{E})$ curve contains also information on the electronic structure of unoccupied bands. This latter feature is held responsible for the enhanced levels around, for instance, 6 $eV^{1/2}$ and around 13 $eV^{1/2}$.

The missing $n = 3$ peak in the $(I, \sqrt{E})$ curves in Fig. 3 is explained by the fact that the extra intensity expected at $\sqrt{E}$ equaling 4.6 $eV^{1/2}$ is counteracted by an expected dip at $\sqrt{E}$ equaling 4.3 $eV^{1/2}$ for resonant scattering involving the (1,1) diffraction channel. This small difference in energy may even explain the minute apparent intensity maximum at $\sqrt{E}$ equaling 5.3 $eV^{1/2}$.

We finally note that the straight line in the inset in Fig. 3 just misses the origin. The fact that we disregarded the energy of the ground state in the image potential is responsible for a shift on the $\sqrt{E}$ scale. A different phase shift for electron scattering from the surface and that from the hidden interface would, however, lead to a shift on the vertical scale. It is impossible to disentangle both features in a credible way.

We analyze the LEEM $(I, \sqrt{E})$ curve in Fig. 3 in terms of Fabry-Pérot interferences in the inset. In line with Eq. (3), a plot on the order of the marked maxima versus $\sqrt{E}$ leads to a straight line with a correlation coefficient of 0.998. From the obtained slope, we find $D = 4.2$ Å and, thus, $d = 0.6$ Å. The smoothness of the β^* interfaces and their stability are attributed to quantum size effects (QSEs). A standing wave of the Fermi electrons leads to a disappearing electron density at the interfaces and, thus, enhanced stability or vice versa lower energy. In a simple-minded view, considering the Ge_3Pt nanosheet as an infinitely deep potential well, the Fermi wavelength would then correspond to 8.6 Å, i.e., twice the width of the potential well. Because the electron spillover for a potential well of finite depth, this value is an underestimate.

We now discuss the requirements for introducing the alloy Ge_3Pt, which is absent in the bulk phase diagram. The first indication for a new phase is the substantial surface smoothening as evident from Figs. 1(a) and 1(b). Such a smoothening is absent for a Ge(011) substrate after deposition of Pt and a subsequent similar high-temperature treatment. This points at the emergence of a new phase with low interface energies. The composition of the deep eutectic $Ge_{1-x}Pt_x$ phase is given by $x = 0.22$ [26]. No stable phases with $x < 0.22$ are known. The bulk binary phase diagram shows on the Pt-rich side of the eutectic point Ge_2Pt, Ge_3Pt_2, GePt,..., as stable alloys. Indeed, cooling through the eutectic point of a Pt-covered Ge(110) surface leads to spinodal decomposition into clean Ge(110) and the precipitation of Ge_2Pt hut clusters [27]. The first option, i.e., to form Ge_3Pt entities is obviously passed since this material is thermodynamically unstable as a bulk material. In the current case, QSEs appear to push the subtle thermodynamic balance towards a stable Ge_3Pt nanophase. Since the QSE-induced energy gain per atom eventually diminishes with growing thickness of the Ge_3Pt film, the finding is perfectly consistent with its absence in the bulk phase diagram. The importance of QSE grows with an increasing probability for specular scattering of the Fermi electrons at the buried interface and at the surface. This probability is high for Ge(001) [and low for Ge(110)] and is further enhanced by the observed smoothening of the Pt-Ge surface as observed experimentally. Since Ge_3Pt does not exist in a bulk form, structural information is not available since a tool with sufficient spatial and composition information has yet to be invented. Still, we know that the in-plane atomic density has to be half that of Ge(001) because of the (1×2) reconstruction and the obtained interplanar distance is 0.6 Å. The atomic density within the Ge_3Pt nanosheet amounts, then, to 5.15×10^{22} cm^{-3}, i.e., similar to that of germanium (4.42×10^{22} cm^{-3}). With an approximate carrier density of about 10^{22} cm^{-3} (determined using the Fermi wavelength), Ge_3Pt behaves like a metal.

The Ge_3Pt nanofilm can be modeled with an asymmetric potential well. The Fermi electrons in the Ge_3Pt layer experience a barrier height equal to the work function of Ge_3Pt at the vacuum/Ge_3Pt interface. From our LEEM I(V) measurements, we extract a work function of about 1.75 eV. The second barrier that the Fermi electrons in the Ge_3Pt layer experience is located at the interface between the Ge_3Pt layer and the Ge(001) substrate and is a sizable portion of the Ge band gap. Due to the negative excess charge at the Ge_3Pt/Ge(001) interface, the energy bands of Ge are strongly bent upwards, and we expect the barrier to be similar to the band gap of Ge, i.e., about 0.67 eV. The energy eigenvalues $E = \frac{\hbar^2 k^2}{2m}$ of the asymmetric one-dimensional well can be found by solving the transcendental equation [28],

$$kD = n\pi - \arcsin\left(\frac{\hbar k}{\sqrt{2mV_1}}\right) - \arcsin\left(\frac{\hbar k}{\sqrt{2mV_2}}\right), \quad (4)$$

where D is the layer thickness, m is the mass of the Fermi electron, and k is the momentum of the electron. $n = 1$–3, and $V_{1,2}$ are the potential barriers at the Ge_3Pt-vacuum interface (1.75 eV) and the Ge_3Pt-Ge interface (0.67 eV), respectively. Here, we consider the Fermi electrons in the Ge_3Pt layer, which have a Fermi wavelength $\lambda_F = \frac{2\pi}{k_F}$. The first ($n = 1$) quantum stabilized layer thickness $D = 0.42$ nm, results in a Fermi wavelength of 1.71 nm. The difference with the previously mentioned underestimate of 0.84 nm is mainly due to spillover of the wave function at both shallow barriers. We cannot exclude that effects due to effective masses also play a role here.

The exact composition of the PiNWs hosted on the Ge_3Pt phase is still unresolved. Ample circumstantial experimental evidence was reported to suggest that they most likely consist of Pt atoms [11–14]. Density functional theory [29] results would indicate that the constituting dimers consist of Ge. However, this 0-K result is incompatible with the observed (4×4) structure at low temperatures [11]. Some recent papers favor Ge dimer rows [30,31]. The present data shed some new light on this issue. Upon cooling down through the eutectic temperature, first a (2×1) μLEED pattern emerges at 1004 K, which demonstrates the solidification of the Ge_3Pt phase. It is only at a no less than 360 K (!) lower temperature that the occurrence of the $c(4 \times 2)$ phase reveals the emergence of PiNWs. At 360 K below the eutectic temperature, this obviously cannot be attributed to spinodal decomposition anymore but is rather indicative of (partial) segregation of either Pt or Ge from the Ge_3Pt(001) thin film.

IV. CONCLUSIONS

In conclusion, heating of a Pt-covered Ge(001) surface leads to the evolution of a eutectic phase. Subsequent slow cooling through the eutectic point (at about 1004 K) results in a dramatically smoothened surface with a more than ten times enlarged average terrace width compared to that of the clean surface as revealed by LEEM. The measured intensity versus energy curve shows a rich pattern of intensity maxima and minima. The minima are attributed to bound-state resonances of the probing electrons, including the most prominent one at E equaling 9.4 eV. This dip is related to resonant diffraction of the electrons into channels involving a periodicity of 4.00 Å, i.e., equal to the Ge-Ge nearest-neighbor distance. This provides a straightforward and accurate way to calibrate the intrinsic energy scale. We obtain a perfectly linear relationship between the order of the intensity peaks and the square root of their energy. This reveals Fabry-Pérot interference between reflection of the probing electrons at the exposed and buried interfaces. All observations are consistently explained by the evolution of a QSE-stabilized Ge_3Pt nanosheet, which evolves during spinodal decomposition of the eutectic phase during cooling. This new nanosized phase consists of eight layers. The PiNWs form probably as a result of segregation and restricted 2D mobility at 641 K and below. Our data confirm that phases do exist on the nanoscale which are not stable in macroscopic dimensions. It also stresses the urgency to obtain more in-depth information for a detailed understanding of thin films. These findings apply for an important class of surface-confined alloys.

ACKNOWLEDGMENTS

We gratefully acknowledge financial support from the Netherlands Organization for Scientific Research (NWO).

[1] J. Wan, Y. L. Fan, D. W. Gong, S. G. Shen, and X. Q. Fan, Surface relaxation and stress of fcc metals: Cu, Ag, Au, Ni, Pd, Pt, Al and Pb, Modell. Simul. Mater. Sci. Eng. **7**, 189 (1999) and references therein.

[2] K. Oura, V. G. Lifshits, A. Saranin, A. V. Zotov, and M. Katayama, *Surface Science: An Introduction* (Springer, Berlin, 2003).

[3] B. Ressel, K. C. Prince, S. Heun, and Y. Homma, Wetting of Si surfaces by Au-Si liquid alloys, J. Appl. Phys. **93**, 3886 (2003).

[4] S. Kodambaka, J. Tersoff, M. C. Reuter, and F. M. Ross, Germanium nanowire growth below the eutectic temperature, Science **316**, 729 (2007).

[5] O. G. Shpyrko, R. Streitel, V. S. K. Balagurusamy, A. Y. Grigoriev, M. Deutsch, B. M. Ocko, M. Meron, B. Lin, and P. S. Pershan, Surface crystallization in a liquid AuSi alloy, Science **313**, 77 (2006).

[6] O. G. Shpyrko, R. Streitel, V. S. K. Balagurusamy, A. Y. Grigoriev, M. Deutsch, B. M. Ocko, M. Meron, B. Lin, and P. S. Pershan, Crystalline surface phases of the liquid Au-Si eutectic alloy, Phys. Rev. B **76**, 245436 (2007).

[7] A. L. Pinardi, S. J. Leake, R. Felici, and I. K. Robinson, Formation of an Au-Si eutectic on a clean silicon surface, Phys. Rev. B **79**, 045416 (2009).

[8] O. Gürlü, O. A. O. Adam, H. J. W. Zandvliet, and B. Poelsema, Self-organized, one-dimensional Pt nanowires on Ge(001), Appl. Phys Lett. **83**, 4610 (2003).

[9] H. J. W. Zandvliet, A. van Houselt, and B. Poelsema, Self-lacing atomic chains, J. Phys.: Condensed Matter **21**, 474207 (2009).

[10] N. Oncel, A. van Houselt, J. Huijben, A.-S. Hallbäck, O. Gürlü, H. J. W. Zandvliet, and B. Poelsema, Quantum Confinement between Self-Organized Pt Nanowires on Ge(001), Phys. Rev. Lett. **95**, 116801 (2005).

[11] A. van Houselt, T. Gnielka, J. M. J. Aan de Brugh, N. Oncel, D. Kockmann, R. Heid, K.-P. Bohnen, B. Poelsema, and H. J. W. Zandvliet, Peierls instability in Pt chains on Ge(001), Surf. Sci. **602**, 1731 (2008).

[12] A. Safaei, B. Poelsema, H. J. W. Zandvliet, and R. van Gastel, Spinodal decomposition driven formation of Pt-nanowires on Ge(001), New J. Phys. **16**, 113052 (2014).

[13] N. Oncel, W. J. van Beek, J. Huijben, B. Poelsema, and H. J. W. Zandvliet, Diffusion and binding of CO on Pt nanowires, Surf. Sci. **600**, 4690 (2006).

[14] A. Saedi, R. P. Berkelaar, A. Kumar, B. Poelsema, and H. J. W. Zandvliet, Adsorption of Cu phthalocyanine on Pt modified Ge(001): A scanning tunneling microscopy study, Phys. Rev. B **82**, 165306 (2010).

[15] O. Gürlü, H. J. W. Zandvliet, B. Poelsema, S. Dag, and S. Ciraci, Initial stages of Pt growth on Ge(001) studied by scanning tunneling microscopy and density functional theory, Phys. Rev. B **70**, 085312 (2004).

[16] E. Bauer, Low energy electron microscopy, Rep. Prog. Phys. **57**, 895 (1994).

[17] R. M. Tromp and M. C. Reuter, Step morphologies on small-miscut Si(001) surfaces, Phys. Rev. B **47**, 7598 (1993).

[18] E. van Vroonhoven, H. J. W. Zandvliet, and B. Poelsema, $(2 \times 1) - (1 \times 1)$ Phase Transition on Ge(001): Dimer Breakup and Surface Roughening, Phys. Rev. Lett. **91**, 116102 (2003).

[19] A. Safaei, An *in-situ* low-energy electron microscopy study of Pt- and Au-induced modifications of Ge(001), Ph.D. thesis, University of Twente, 2015.

[20] B. Poelsema, M. S. Altman, R. van Gastel, H. J. W. Zandvliet, and A. van Houselt, Ordinary and supernumerary resonant scattering of low energy electrons from the $BiCu_2(111)$ surface alloy, New J. Phys. **19**, 013024 (2017).

[21] M. S. Altman, W. F. Chung, and C. Liu, LEEM phase contrast, Surf. Rev. Lett. **05**, 1129 (1998).

[22] W. F. Chung, Y. J. Feng, H. C. Poon, C. T. Chan, S. Y. Tong, and M. S. Altman, Layer Spacings in Coherently Strained Epitaxial Metal Films, Phys. Rev. Lett. **90**, 216105 (2003).

[23] M. S. Altman, W. F. Chung, Z. Q. He, H. Poon and S. Y. Tong, Quantum size effect in low energy electron diffraction of thin films, Appl. Surf. Sci. **169**, 82 (2001).

[24] T. R. J. Bollmann, R. van Gastel, H. J. W. Zandvliet, and B. Poelsema, Quantum Size Effect Driven Structure

Modifications of Bi Films on Ni(111), Phys. Rev. Lett. **107**, 176102 (2011).

[25] T. R. J. Bollmann, R. van Gastel, H. J. W. Zandvliet, and B. Poelsema, Quantum size effects on surfaces without a projected bandgap: Pb/Ni(111), New J. Phys. **13**, 103025 (2011).

[26] Y. Oya and T. Suzuki, The platinum-germanium phase diagram, Z. Metallkd. **78**, 295 (1987).

[27] R. van Bremen, P. Bampoulis, J. Aprojanz. M. Smithers, B. Poelsema, C. Tegenkamp, and H. J. W. Zandvliet, Ge_2Pt hut clusters: A substrate for germanene, J. Appl. Phys. **124**, 125301 (2018).

[28] L. D. Landau and E. M. Lifshitz, *Quantum Mechanics: Non-Relativistic Theory* (Butterworth-Heinemann, Oxford, 2013).

[29] D. E. P. Vanpoucke and G. Brocks, Formation of Pt-induced Ge atomic nanowires on Pt/Ge(001): A density functional theory study, Phys. Rev. B **77**, 241308(R) (2008).

[30] E. Inami, Y. Sugimoto, T. Shinozaki, O. Gurlu, and A. Yurtsever, Investigation of atomic species in Pt-induced nanowires on Ge(001) surface by combined atomic force and scanning tunneling microscopy, Phys. Rev. B **96**, 155415 (2017).

[31] S.-F. Tsay, Pt-chain induced formation of Ge nanowires on the Ge(001) surface, Surf. Sci. **606**, 1405 (2012).